Pivotal role of RIP1 and MLKL in neuronal cell death induced by the human neuroinvasive coronavirus OC43

Mathieu MEESSEN-PINARD[1], Alain LE COUPANEC[1],
Marc DESFORGES[1#] and Pierre J. TALBOT[1#]

[1]*Laboratory of Neuroimmunovirology, INRS-Institut Armand-Frappier, Université du Québec, Laval, Québec, Canada*

Running title: RIP1&MLKL-dependent neuron death after HCoV infection

Keywords: Coronavirus, Human Coronavirus, Human Coronavirus OC43, Regulated cell death, Necroptosis, RIP

Word count: Abstract: 225 words Text: 7 147 words

Co-correspondent footnote:

Dr. Pierre J. Talbot
Laboratory of Neuroimmunovirology
INRS-Institut Armand-Frappier
531, boulevard des Prairies
Laval (Québec) H7V 1B7
Canada

Tel.: (450) 687-5010 extension 4300
Fax: (450) 686-5501
E-mail: pierre.talbot@iaf.inrs.ca

Dr. Marc Desforges
Laboratory of Neuroimmunovirology
INRS-Institut Armand-Frappier
531, boulevard des Prairies
Laval (Québec) H7V 1B7
Canada

Tel.: (450) 687-5010 extension 4342
Fax: (450) 686-5501
E-mail: marc.desforges@iaf.inrs.ca

ABSTRACT

Human coronaviruses (HCoV) are respiratory pathogens with neuroinvasive, neurotropic and neurovirulent properties, highlighting the importance to study the potential implication of these viruses in neurological diseases. The OC43 strain (HCoV-OC43) was reported to induce neuronal cell death which may participate in neuropathogenesis. Here, we show that HCoV-OC43 harboring two point mutations in the spike glycoprotein (rOC/$U_{s183-241}$) was more neurovirulent than the wild-type HCoV-OC43 (rOC/ATCC) in mice and induced more cell death in murine and human neuronal cells. To evaluate the role of regulated cell death (RCD) in HCoV-OC43-mediated neural pathogenesis, we determine if knockdown of Bax, a key regulator of apoptosis, or RIP1, a key regulator of necroptosis, altered the percentage of neuronal cell death following HCoV-OC43 infection. We found that Bax-dependent apoptosis did not play a significant role in RCD following infection, as inhibition of Bax expression mediated by RNA interference did not confer cellular protection against the cell death process. On the other hand, we demonstrated that RIP1 and MLKL were involved in neuronal cell death as RIP1 knockdown and chemical inhibition of MLKL significantly increased cell survival after infection. Taken together, these results indicate that RIP1 and MLKL contribute to necroptotic cell death after HCoV-OC43 infection to limit viral replication. However, this RCD could lead to neuronal loss in the mouse CNS and accentuate the neuroinflammation process reflecting the severity of neuropathogenesis.

IMPORTANCE OF THE STUDY

Because they are naturally neuroinvasive and neurotropic, human coronaviruses are suspected to participate in the development of neurological diseases. Given that the strain OC43 is neurovirulent in mice and induces neuronal cell death, we explored the neuronal response to infection by characterizing the activation of RCD. Our results revealed that classical apoptosis associated with the Bax protein is not playing a significant role in HCoV-OC43-induced neuronal cell death and that RIP1 and MLKL, two cellular proteins usually associated with necroptosis (a RCD back-up system when apoptosis is not adequately induced), both play a pivotal role in the process. As necroptosis disrupts cellular membranes and allows the release of damage-associated molecular patterns (DAMP) and may induce the production of pro-inflammatory cytokines, it may represent a pro-inflammatory cell death mechanism that contributes to excessive neuroinflammation and neurodegeneration and eventually to neurological disorders after a coronavirus infection.

INTRODUCTION

Human coronavirus (HCoV) are largely associated with common cold whereas elders, newborns, infants or immune-compromised individuals are more susceptible to develop severe lower respiratory infection such as pneumonia or bronchitis (1). Over the years, evidence has accumulated to support the idea that HCoV can act as opportunistic pathogens that can be associated with other pathologies, including neurological disorders (2-6). Moreover, HCoV-OC43 has recently been detected in the brain of an immunodeficient child who died from fatal encephalitis (7).

Like its murine counterpart, mouse hepatitis virus (MHV), which is recognized to induce neurological disorders in mice models (8, 9), we have previously demonstrated that the human coronavirus strain OC43 (HCoV-OC43) possesses neuroinvasive and neurotropic properties that allow the virus to invade, spread and persist within the murine central nervous system (CNS) where neurons represent the main target during the acute phase of infection (10, 11). Furthermore, HCoV-OC43 is also naturally neuroinvasive in humans as RNA was detected in human brain samples of patient suffering neurological diseases such as Alzheimer's, Parkinson's disease, multiple sclerosis and in controls (12). Furthermore, we have previously demonstrated that HCoV-OC43 has the capacity to induce neuronal cell death (11, 13) associated with the induction of the unfolded protein response (UPR) and ER stress, as well as degeneration of neurons (13-17). However, the exact underlying mechanism of neuronal cell death induced during HCoV-OC43 infection remains poorly understood and its involvement in neuropathogenesis is still unclear.

Regulated cell death (RCD) represents a large homeostasis system that controls several aspects of a cell life (18). One of these roles may be considered as a defense

mechanism against viral infection in order to control or limit propagation and protect the entire organism (19, 20). Different RCD pathways are now identified based on biochemical features in order to improve our understanding of cell response to stress (21). The most known and studied form of RCD is caspase-dependent apoptosis, characterized by extracellular stress signals sensed by receptors (extrinsic apoptosis) or intracellular stress (intrinsic apoptosis), which activates specific cellular factors, including caspase-8 and the pro-apoptotic Bax protein that converge to trigger activate downstream effector caspases (22-24). More recently, necroptosis, another form of RCD, has gained attention as this regulated necrosis independent of caspases can act to replace classical apoptosis pathways (25). Necroptosis often involves attachment of TNFα to its receptor (TNFR1) on the cell surface, which can induce a downstream death signal characterized by a core component composed of receptor-interacting protein kinase 1 (RIP1) and RIP3 interacting with each other (26). In the case where caspase-8 activity is somehow abrogated, RIP1 can interact with RIP3 and the complex is activated by phosphorylation (27-30). The RIP1-RIP3 complex then participates in the cell-membrane disruption mediated by the phosphorylated form of mixed lineage kinase domain-like (MLKL) and ultimately in cell death (31-33).

In the present study, we sought to further investigate the underlying mechanisms of HCoV-OC43-induced neuronal cell death after infection, by identifying cellular factors involved in the different pathways associated with RCD and their potential association with neuropathogenesis during a CNS infection. Overall, the global portrait suggests that Bax-dependent apoptosis is not significantly involved during infection of human neuronal cells by HCoV-OC43, but that necroptosis, which involves RIP1 and MLKL, seems to

play a central role in the regulation of neuronal cell death in order to limit viral replication and propagation.

MATERIALS AND METHODS

Ethics and biosafety statement. All animal experiments were approved by the Institutional Animal Care and Use Ethics Committee (IACUC) of the *Institut national de la recherche scientifique* (INRS) and conform to the Canadian Council on Animal Care (CCAC). Animal care and used protocols numbers 1304-02 and 1205-03 were issued by the IACUC of INRS for the animal experiments described herein. All the experiments with both wild-type and mutant viruses (S protein with a potential gain-of-function) were approved by the institutional biosafety committee (IBC) at INRS (certificate 2013-07) as all BSL2 safety level measures were applied to prevent infection of all laboratory workers and potential spread of viruses.

Cell lines, viruses and reagents. The human neuroblastoma LA-N-5 cell line (a kind gift from Dr Stephan Ladisch, George Washington University School of Medicine, USA) was routinely cultured at 37°C with 5% CO_2 in RPMI (Life Technologies) supplemented with 15% (vol/vol) of fetal bovine serum (FBS, GE Healthcare), 10 mM HEPES, 1 mM Sodium Pyruvate (NaPy) and 100 µM nonessential amino acids (Life Technologies). The LA-N-5 cells were differentiated into neurons as previously described (13, 34) for all experiments. Briefly, cells were seeded in RPMI supplemented with 15% (vol/vol) FBS, 10 mM HEPES, 1 mM NaPy, 100 µM non-essential amino acids and the next day and every two days for a period of 6 days, 10 µM all-trans retinoic acid (Sigma-Aldrich) was added to the same medium supplemented with 10% (vol/vol) of FBS. The HRT-18 cells (kind gift from the late David Brian, University of Tennessee) were

cultivated in minimal essential medium alpha (MEM-alpha, Life Technologies) supplemented with 10% (vol/vol) FBS.

The recombinant wild-type (wt) reference HCoV-OC43 (rOC/ATCC) virus and the recombinant mutant HCoV-OC43 virus (rOC/$Us_{183-241}$), containing two point mutations within the S spike glycoprotein (H183R and Y241H), were generated using full-length cDNA clone as previously described (13, 35). LA-N-5 cells were infected at a multiplicity of infection (M.O.I.) of 0.2 during two hours at 37°C for adsorption and then incubated with RPMI supplemented with 2.5% (vol/vol) FBS for indicated time post-infection. For infection of LA-N-5 cells with the wild-type Indiana strain of Vesicular Stomatis Virus (VSV), a MOI of 1 was used and viruses were incubated in a minimal volume for 1h at 37°C. The media was replaced by RPMI with 2.5 % (vol/vol) FBS and then cells were incubated at the indicated times.

Staurosporine (STS) was purchased from Sigma-Aldrich and used to treat LA-N-5 cells at a final concentration of 500 nM and incubated overnight at 37°C. Necrosulfonamide (NSA) was purchased from Abcam and used at 2 µM.

Mice, survival curve, body weigh variation and evaluation of clinical scores. Twenty-two day-old female BALB/c mice (Charles River) were inoculated by the intracerebral route with $10^{2,5}$ Tissue Culture Infective Dose $(TCID)_{50}$ of wt or mutant virus, as previously described (17). Groups of 10 mice were subjected to observation on a daily basis for survival and body weight variations over a period of 22 days post-infection. Clinical scores were evaluated using a scale with 4 distinctive levels, as previously described (36). Briefly, asymptomatic mouse were classified as number 0; 1 for mice symptoms of abnormal flexion of the four limbs; 2 for mice presenting social isolation,

ruffled fur and hunched backs and number 3 was attributed to mice that were in moribund state or dead.

Primary cultures of mouse CNS. Embryos at 14 to 16 days of gestation were removed from pregnant anesthetized CD1 mice. The cortex and hippocampus of the embryonic pup brains were harvested and placed in Hanks balanced salt solution (HBSS) medium, without Ca^{2+} and Mg^{2+}, supplemented with 1.0 mM sodium pyruvate and 10 mM HEPES buffer. The tissues were incubated in 5 ml of solution of HBSS and trypsin-EDTA 0.5% (ratio 10:1 respectively) for 15 min at 37°C with gentle tilting to mix. After digestion, the tissues were washed 5 minutes three times with HBSS, and the medium was removed and replaced by fresh HBSS medium (without Ca^{2+} and Mg^{2+}, supplemented with 1.0 mM sodium pyruvate and 10 mM HEPES buffer). Tissues were gently pipetted up and down with a Pasteur pipette to dissociate the cells. After a decantation step of 5 min at room temperature, supernatants were then transferred into a 50 ml tube with 36 mL of neurobasal medium (Life Technologies) supplemented with 0.5 mM GlutaMAX-I (Life Technologies), 10 mM HEPES buffer, B27 supplement (Life Technologies), gentamycin and 10% of Horse serum. This step was realized twice to increase the final amount of cells. Cells were then seeded at approximately $1x10^5$ cells/cm^2 and grown on collagen-poly-D-lysine (3:1 for a final concentration at 50µg\mL)-treated glass coverslips for immunofluorescence assay in the same medium, which was replaced by fresh neurobasal medium without horse medium the next day. The medium was changed every 2 days after and the cultures were ready for infection after 7 days in culture. For experiments where RNA/proteins or virus was harvested, cells were seeded without glass coverslips in 24 or 6-well plates respectively.

Cell viability assay. Cell viability of LA-N-5 cells was monitored using PrestoBlue (Life Technologies) through reduction of resazurin-like reagent according to the manufacturer's protocol. Briefly, cells were plated at $2.5x10^3$ per well, grown and differentiated with all-trans retinoic acid (Sigma-Aldrich) in Cell+ 96-well plates (Starstetd). After indicated time post-infection, PrestoBlue was added in each well and optical density read as substraction from 570nm-600nm every hour for three hours with a microplate reader (Bio-Rad). Cell viability was determined according to slope regression analysis for each sample and compared to the slope from mock-infected cells. Cell viability of murine primary cultures of CNS was monitored using the reduction of 3-(4,5-dimethylthiazol-2-yl)-2,5-diphenyltetrazolium bromide dye (MTT assay) following the manufacturer's instruction (Roche). Briefly, after indicating time post-infection, 50 µl of MTT labeling reagent were added in primary cultures of mouse CNS seeded in 24-well plates containing 500 µl of NeuroBasal medium. After incubation of cells at 37°C for 1 h, 550 µl of MTT solubilisation buffer were added in each wells and then incubated at 37°C for 18 h. From each well of the 24-well plate, 200 µl were transferred in 5 new wells of 96-well plates and the OD was measured in replicates at 570 nm using a microplate readers (Bio-rad).

Quantification of infectious virus production by IPA. Indirect immunoperoxydase assay (IPA) was performed to evaluate viral production as free virus (in the cell culture medium) and as cell-associated virus, as previously described (37). Briefly, serial dilution of infected LA-N-5 cells supernatant (free virus) or frozen/thawed whole cell lysates (cell-associated virus) were added on HRT-18 cells seeded in 96-well plates and incubated at 37°C with 5% CO_2 for four days. The cells were washed once with

PBS and fixed with methanol containing 0.1% v/v hydrogen peroxide. The primary antibody was the mouse mAb 4.3E4 (1/2) added to each well to detect viral S glycoprotein and incubated at 37°C with 5% CO_2 for two hours then washed three times with PBS. The cells were then incubated with the goat anti-mouse secondary antibody (KPL) conjugated with horseradish peroxidase at 37°C without CO_2 for two hours and washed again with PBS three times. Immune complexes were detected with 0.2 mg/ml of 3,3'-diaminobenzidine tetrahydrochloride (DAB) (Sigma-Aldrich) and 0.01% hydrogen peroxide (H_2O_2) in PBS. Viral titers were analyzed by the Karber method, as previously described (37).

RNA extraction, cDNA synthesis and quantitative PCR. Total RNA from cells was extracted using the RNeasy Mini Kit (Qiagen) according to the manufacturer's protocol. Total RNA quantification was determined using a Nanodrop N-1000 Spectrophotometer (Thermo Scientific) and cDNA synthesis was performed using the Superscript III First-Strand kit (Life Technologies) with 2 µg of RNA according to the manufacturer's instructions. Detection and quantification of gene expression of each gene of interest were performed using specific primers and the SsoFast EvaGreen Supermix (BIORAD). PCR products were detected and quantified using the Rotor-Gene 6000 quantitative real-time PCR (qPCR) instrument (Corbett Life Science).

Protein extraction and Western Immunoblotting. Total proteins were extracted from whole cell lysates in Petri dishes (cells kept on ice) with cell scraper (Sarstedt) and washed with 5 ml of PBS. Cells were centrifuged at 3500 rpm for 5 min at 4°C and washed once with 1 ml of PBS. The cells were transferred to a microtube and centrifuged again at 3500 rpm for 5 min at 4°C and the pellet was resuspended in RIPA buffer (0.15

mM NaCl, 1% (vol/vol) Nonidet P-40, 0.5% (wt/vol) deoxycholate, 0.1% (wt/vol) SDS and 0.05 M Tris pH 8.0) containing fresh Protease inhibitor cocktail set I (Calbiochem). Cell lysates were incubated on ice for 20 minutes and centrifuged at 14 000 rpm for 10 minutes at 4°C. The supernatants were transferred to a new tube and conserved at -80°C for further analysis.

Protein concentrations were measured using the bicinchoninic acid (BCA) protein assay kit (Novagen) according to the manufacturer's protocol. Equal amounts of proteins were subjected to Sodium Dodecyl Sulfate-polyacrylamide gel electrophoresis (SDS-PAGE) using 10% or 4-15% Criterion XT Precast gels (BIORAD) and then transferred to Polyvinyl difluoride (PVDF) membrane (Bio-Rad) with a trans-Blot semidry transfer cell apparatus. The membranes were blocked for one hour at room temperature (RT) with 5% wt/vol skim fat milk in Tris-Buffered saline containing 0.1% (vol/vol) Tween 20 (TBS-T) and incubated with TBS-T containing primary antibodies with 5% (wt/vol) skim fat milk at 4°C overnight. Western blots were performed for detection of Bax, RIP1, RIP3 and Glyceraldehyde-3-phosphate dehydrogenase (GAPDH) proteins using rabbit anti-human Bax antibody (1/2000; sc-493, Santa Cruz Biotech), mouse anti-human/mouse RIP1 antibody (1/2000; clone38, BD Biosciences), rabbit anti-human RIP3 antibody (1/2000; 27-361, ProSci) and rabbit anti-human GAPDH antibody (1/10 000; sc-25778, Santa Cruz Biotech) as primary antibodies respectively. The membranes were washed three times with TBS-T at RT for 5 min before being incubated with anti-mouse or anti-rabbit secondary antibodies (GE Healthcare) coupled to horseradish peroxidase (HRP) for 1 h at RT. After three washes, the bands were visualized by chemiluminescence using the Clarity Western ECL substrate (Bio-Rad) and loading was normalized to the housekeeping protein GAPDH.

Lentivirus production, transduction, overexpressing clones and generation of knock-down LA-N-5 cell populations. Lentiviral pseudoparticles used for gene silencing were produced following transfection of HEK293T cells with pLP1, pLP2, pVSV-G (Sigma-Aldrich) and short hairpin RNA (shRNA) vectors. The Mission pLKO.1 shRNA vector against Bax (shRNA #1: TRCN0000312626, shRNA #2: TRCN0000312627), RIP1 (shRNA #1: TRCN00000705, shRNA #2: TRCN00000709) and the control shRNA (non-target shRNA) were purchased from Sigma-Aldrich. Overall, $5x10^6$ cells were plated in petri dishes pre-coated with sterile PBS containing gelatin 0.1% (vol/vol). Then, cells were co-transfected with 6 µg of each vectors per petri dish and Lipofectamine 3000 (Life Technologies) according to manufacturer's protocol. After 5 h, the medium was replaced by DMEM supplemented with 10% (vol/vol) FBS and then incubated for 96 h at 37°C with 5% CO_2. The supernatant was harvested and lentiviral pseudoparticles were concentrated using the Lenti-X Maxi Purification Kit (Clontech) before being purified and eluted in sterile PBS with PD-10 columns according to manufacturer's protocol (GE Healthcare).

For the transient knock-down of RIP1 expression, LA-N-5 cells were differentiated into neurons with retinoic acid for 6 days and lentiviral pseudoparticules were added to a MOI of 10. After 24 h, the medium was replaced with RPMI containing retinoic acid to complete the differentiation and the cells were incubated for another 48 h before proceeding to infection with HCoV-OC43.

For stable Bax knock-down, undifferentiated LA-N-5 cells were transduced with Bax lentiviral pseudoparticles and cell populations were selected with 2 µg/ml puromycin after 24h in RPMI supplemented with 20% (vol/vol) FBS. A population of LA-N-5 cells

transduced with empty vector (EV) selected as previously described were used as reference cells. All populations of Bax knock-down LA-N-5 cells were maintained in RPMI 15% FBS supplemented with 1 µg/ml puromycin during all experiments. The expression level of Bax in all populations was analyzed by qPCR and western blots.

Immunofluorescence/Immunohistochemistry. For immunofluorescence assay, cells were washed with sterile PBS then fixed with 4% wt/vol paraformaldehyde (PFA, Fisher) for 30 min at RT. After another washing with PBS, cells were permeabilized with 100% methanol at -20°C for 5 min and washed once again with PBS. Cells were incubated with different primary antibodies: mouse anti-spike HCoV-OC43 protein (1-10.C3) monoclonal antibody (1/2; hybridoma supernatant), polyclonal rabbit anti-S protein of the bovine coronavirus (BCoV; 1/1000), monoclonal mouse anti-microtubule-associated protein 2 (MAP2) antibody (1/1000; 556320, BD Biosciences), polyclonal rabbit anti-glial fibrillary acidic protein (GFAP) antibody (1/1000; Z0334, Dako), rabbit anti-MLKL (1/200; M6687, Sigma-Aldrich) or rabbit anti-phosphorylated MLKL (1/200; EPR9514, Abcam) for 1 hour at RT and then washed three times with PBS. Cells were incubated for 1 hour at RT with secondary antibodies (Life Technologies) anti-mouse AlexaFluor 488 (1/1000), anti-rabbit AlexaFluor 488 (1/1000), anti-mouse AlexaFluor 647 (1/1000) or anti-mouse AlexaFluor 568 (1/1000) and then washed three times with PBS. Nucleus were detected with 4', 6'-diamidino-2-phenyl-indole (DAPI) for 5 min at RT and washed once with PBS. For experiments of non-permeabilized LA-N-5 cells, antibodies were diluted in cold media (RPMI 5% FBS) and added on chilled cells on ice for 1 hour before been washed twice with cold media. Then, ice-cold cells were incubated with secondary antibody diluted in cold media for 1 hour, washed and fixed in PFA 4% for 20 min at RT.

For Immunohistochemistry (IHC), mice infected (wt or mutant virus) or not (sham) were perfused with 4% wt/vol PFA and whole brain were carefully harvested from mice infected at 5, 7 and 9 days after intracerebral injection of each virus. Brain tissues were sectioned using a vibratome (VT1000E, Leica) to yield 60-µm sections. Prior to staining, sections were incubated with a solution of two droplets of H_2O_2 in PBS for 10 min at RT and washed with PBS. Sections were then blocked with a solution of PBS containing 1 droplet of horse normal serum according to the manufacturer's protocol (ABC kit Vectastain, Vector Laboratories) for 1 hour at RT. Tissue sections were incubated with primary antibodies for detection of N protein (1/1000; ascites fluid of the 4-E11.3 hybridoma) and activated astrocytes (1/1000; rabbit anti-glial fibrillary acidic protein antibody (GFAP), Dako) overnight at 4°C. Tissue sections were washed with PBS three times and then incubated with secondary biotinylated antibody against mouse immunoglobulin G before revealing with ABC Vectastain kit.

Statistical analysis. Statistical analysis was performed using SimStat or XLSTAT software. Data are represented as mean ± SD. For experiments on mice, statistical significance for survival curves was analyzed using Keplan-Meier followed by a post-test Log-rank (Mantel-Cox) and weight variation was analyzed with Kruskal-Wallis followed by Tukey's post hoc test. For cell experiments, statistical analysis were conducted by student T test or one-way analysis of variance (ANOVA) followed by Tukey's post hoc test.

RESULTS

rOC/U$_{s183-241}$ is more neurovirulent than rOC/ATCC in mice despite a similar production of infectious viral particles in the CNS. We have previously shown that HCoV-OC43 infection leads to human neuronal cell death (13) and that a variant harboring two point mutations in the viral spike (S) glycoprotein (rOC/U$_{s183-241}$) showed a significant increase in virus-induced neuronal cell mortality compared to the reference variant (rOC/ATCC) (14). Some other variants of HCoV-OC43 were shown to have different levels of neurovirulence in infected mice. However, the relationship between neuronal cell death and neurovirulence remains poorly understood. In order to evaluate the neurovirulence of HCoV-OC43, we compared 22-day-old BALB/c mice infected by the intracerebral route (IC) with the wild-type (wt, rOC/ATCC) or the mutant virus (rOC/U$_{s183-241}$), the latter known to increase cell death of the infected human neuronal cell lines LA-N-5 (13). Neurovirulence of both viruses was monitored by survival curves, as already reported (15), but weight loss and clinical scores of neurological symptoms (36) were also evaluated and all these parameters indicated that the S mutant virus rOC/U$_{s183-241}$ was more neurovirulent than the wt virus rOC/ATCC (Fig. 1A-C). Although we observed multiple clinical signs related to encephalitis for both viral infection as seen by social isolation, abnormal flexion of the four limbs, ruffled fur and hunched back, most of all mice infected by the mutant virus presented four levels of clinical scores more rapidly (Fig. 1C) and eventually a higher mortality rate compared to mice infected by the reference virus. To determine whether the difference in neurovirulence observed between rOC/U$_{s183-241}$ and rOC/ATCC was related to viral replication in the CNS, we measured infectious viral particles in brain and spinal cord every 2 days over a period of 22 days

(Fig. 1D). Titers of infectious particles in the brain were the same for both viruses although rOC/$U_{s183-241}$ could be cleared more rapidly than the wild-type virus as observed at 9 dpi (Fig. 1D, left panel). Similar to the brain, infection of the spinal cord by both viruses resulted in a similar production of viral particles, however the mutant virus replicated more rapidly in the spinal cord (Fig. 1D, right panel). Altogether, these results indicate that rOC/$U_{s183-241}$ was more neurovirulent than the reference virus in mice infected after IC inoculation.

Viral dissemination and astrocyte activation are more important following rOC/$U_{s183-241}$ infection compared to rOC/ATCC. Hippocampus is one of the first regions where HCoV-OC43 spreads in the mouse CNS (17). Histological examination revealed that rOC/$U_{s183-241}$ reached this portion of the brain faster than rOC/ATCC for which no antigens were observed before 7 dpi (Fig. 2A). The infection with either virus showed similar disseminated pattern in other regions of the brain such as olfactory bulb and cortex (data not shown). As both viruses spread within the CNS, astrogliosis, considered as a marker of inflammation, was also investigated and was detected in the hippocampus (Fig. 2B). Both viruses induced a mild and similar activation of astrocytes at 5 dpi however, unlike the reference virus, infection with the S mutant virus maintained a moderate activation of astrocyte until 7 dpi.

rOC/$U_{s183-241}$ disseminates more rapidly than rOC/ATCC virus in neuronal cell cultures. In order to study the link between the neurovirulent properties and neuronal cell-death induced by either rOC/$U_{s183-241}$ or rOC/ATCC, we compared two neuronal cell culture models. To establish whether the murine mixed primary CNS cultures and human LA-N-5 cells were susceptible at the same rate to the infection between rOC/ATCC and

rOC/$U_{s183-241}$, the kinetics of viral spread were evaluated by immunofluorescence up to 48 hpi (Fig. 3). In murine primary cultures of CNS, the mutant virus spread more rapidly than the wild-type virus in neurons as seen at 16 and 24 hpi (Fig. 3A). Although neurons are the primary target of infection in murine primary cultures, astrocytes were also infected later during infection by both viruses (data not shown). As observed in Fig. 3B, the mutant virus also spread more rapidly than the wt virus in LA-N-5 cells up to 32 hpi, a time when LA-N-5 cultures were almost all infected by rOC/$U_{s183-241}$ compared to approximately only 50% infection by the wt virus. The difference in viral spread is similar to those observed by histological examination in the CNS of infected BALB/c mice (Fig. 2A).

rOC/$U_{s183-241}$ infection increases neuronal cell death in correlation with more infectious particles production. Given that the S-mutant virus was more neurovirulent and was able to spread faster than the wt virus in the mouse CNS and in neuronal cell cultures, we sought to evaluate whether the neuropathogenesis could be related to neuronal cell death. Even though both viruses induced cell death in murine mixed primary cultures of CNS and human LA-N-5 cells, the mutant virus was significantly more cytotoxic compared to wt virus as seen in Fig. 4A and 4B, respectively. The production of infectious viral particles in cell culture medium (free virus) was significantly higher for mutant virus in LA-N-5 cells whereas no difference was observed in primary cultures (Fig. 4C and 4D, upper panel), however, there was a significant increase of cell-associated infectious particles production for rOC/$U_{s183-241}$ compared to rOC/ATCC virus for both types of cell cultures (Fig. 4C and 4D, lower panel). Taken together, these results indicate that for both neuronal cell cultures, the infection with the mutant virus produced more

372 infectious particles that led to an increase in neuronal cell death compared to the infection
373 with the wild-type virus.

374 **Bax-dependent apoptosis does not play a significant role in neuronal cell death**
375 **following HCoV-OC43 infection.** To push further our understanding of the difference in
376 cytotoxicity between viruses (Fig. 4 and ref 14) and to further characterize the neuronal
377 response associated with RCD after infection, we sought to identify which cellular factors
378 were involved in both neuronal cell models and to evaluate their relative importance after
379 infection by either virus. Bax-dependent apoptosis is one of the best described cell death
380 pathway and we have previously reported that Bax was relocalized to mitochondria after
381 HCoV-OC43 infection (14). As the regulation of this pro-apoptotic factor can also be at
382 the transcriptional level (38, 39), we evaluated its mRNA level and found that infection
383 induced a significant increase in Bax gene expression between 48 hpi and 72 hpi for both
384 viruses (Fig. 5A). Infection with the mutant virus led to a significantly higher increase in
385 Bax gene expression compared to the wt virus, which correlated with the induction of a
386 stronger induction of neuronal mortality in both neuronal cell cultures (Fig. 4A and 4B).
387 On the other hand, the level of Bax protein remained stable and did not correlate with the
388 increase in mRNA (Fig. 5B).

389 Since neuronal response to infection led to an increased expression of the Bax gene
390 and mostly because we already showed that the corresponding protein was relocated to the
391 mitochondria (14), we sought to evaluate the role of this factor in neuronal cell death.
392 Interestingly, even the most efficient knockdown of Bax expression (Fig. 6A; population
393 shRNA Bax #1) did not protect LA-N-5 cells from damages induced by rOC/ATCC or
394 rOC/$U_{s183\text{-}241}$ infection at 48 hpi compared to control as seen by the same cytopathic effect

(rounding of cells and loss of axon indicated by arrowheads and arrows respectively) (Fig. 6B, left panels). In order to verify the functionality of the Bax protein, we assessed the morphology of LA-N-5 cells in the presence of staurosporine (STS) or infected by Vesicular Stomatis Virus (VSV), both known to induce apoptosis through a Bax-dependent cell death pathway (40, 41). Knockdown of Bax expression with the shRNA #1 abolished the cytopathic effect induced by STS or VSV as seen at 24 hpi and reduced the retractions of axons and dendrites (Fig. 6B, right panels) whereas the protection of neurons was moderate for population shRNA #2 (mild inhibition of Bax expression) following treatment with STS or VSV (data not shown). In order to quantify the apparent absence of cellular protection in populations infected with rOC/ATCC or rOC/$U_{s183-241}$, we measured cell viability and confirmed that Bax knockdown did not confer any protection against neuronal cell death induced during HCoV-OC43 infection (Fig. 6C) even though this knockdown led to a strong protection against neuronal cell death induced by STS or VSV at 24 hpi in a dose-dependent manner compared to the control population (Fig. 6D). Together, these results indicate that the pro-apoptotic factor Bax seems functional in the LA-N-5 neuronal cells but does not play a significant role in HCoV-OC43-induced neuronal cell death.

HCoV-OC43 infection induces an increase in RIP1 and RIP3 gene expression. To further investigate RCD following coronavirus infection of neuronal cells and again evaluate whether there was a difference between viruses, we explored the possible involvement of receptor-interacting protein kinase 1 and 3 (RIP1 and RIP3) (29, 42) largely associated with necroptosis and potentially involved in neurological diseases or viral infections (43-46). In murine primary cultures of CNS, an increase in RIP1 (Fig. 7A,

upper panel) or RIP3 mRNA (Fig. 7A, lower panel) was detectable at 48 hpi for both viruses compared to mock-infected cultures even though rOC/$U_{s183-241}$ infection tended to transcribe more RIP1 and RIP3 mRNA. On the other hand, there was no significant increase in the level of corresponding proteins following infection with either virus, compared to mock-infected, in murine primary cultures of CNS (Fig. 7C). In LA-N-5 cells, an increase in RIP1 and RIP3 mRNA was observed for mutant infection compared to mock-infected whereas the wild-type virus infection induced a modest increase in RIP1 gene expression only (Fig. 7B). Surprisingly, our results of Western immunoblotting showed that the amount of the RIP1 protein did not increase following wt or mutant infection compared to mock-infected LA-N-5 cells (Fig. 7D) even if the corresponding gene expression was up-regulated at 48 and 72 hpi (Fig. 6B). Similarly to RIP1, RIP3 protein expression was stable during wt or mutant virus infection.

Inhibition of RIP1 and MLKL protects against neuronal cell death induced by both HCoV-OC43 variants and increases viral replication. Given that neuronal response to HCoV-OC43 infection induced an increase in RIP1 gene expression, an observation usually associated with necroptosis (47), we sought to evaluate the importance of this cell death pathway in neuronal cell death and viral production. By using RNAi to knockdown the expression of RIP1, we transduced LA-N-5 cells with two different shRNA (#1 and #2) and quantified the amount of RIP1 mRNA and protein (Fig. 8). Quantitative PCR and Western blot revealed that the shRNA #2 was more efficient to knock-down expression of RIP1 (Fig. 8A). Inhibition of RIP1 by knockdown decreased the HCoV-OC43-induced cell death at 72 hpi in a dose-dependent manner compared to infected LA-N-5 cells transduced with control shRNA (NT) (Fig. 8B). As expected,

inhibition of RIP1 expression protected LA-N-5 cells more efficiently against wt virus infection compared to the mutant infection, as the mortality rate induced by the latter is more important. In addition, to establish if viral replication was affected following cellular protection conferred by RIP1 knockdown, we quantified the production of wt and mutant infectious viral particles. Surprisingly, a significant increase in cell-associated mutant infectious particles production was observed at 48 and 72 hpi when RIP1 expression was reduced (Fig. 8C). In fact, in the LA-N-5 cells transduced with the most efficient shRNA to knockdown RIP1 expression (shRNA #2), almost 50-fold more rOC/ATCC particles and 100-fold more rOC/$U_{s183-241}$ particles were harvested compared to cells that have been transduced by non-target shRNA. Thus, these results indicate that a reduction of RIP1 expression delayed neuronal cell death induced by both viruses allowing an increase in the production of cell-associated infectious viral particles.

To further describe the cascade of events possibly associated with necroptosis and involving RIP1 during neuronal cell death induced by HCoV-OC43, we studied the activation of the factor Mixed Lineage Kinase domain-like (MLKL), a known downstream effector that act as an ion channel, which disturbs the osmotic homeostasis and disrupts the integrity of plasma membrane (32, 48). Necrosulfonamide (NSA), a chemical inhibitor of MLKL, significantly increased the survival of LA-N-5 cells infected by either virus suggesting a role of MLKL in neuronal cell death induced by HCoV-OC43 (Fig. 9A). Following infection of LA-N-5 cells by the mutant virus, NSA increased survival up to 86% compared to DMSO-treated cells, for which viability was only 44.5%. Inhibition of MLKL also protected cells against mortality during infection with the reference virus by increasing viability by 30% compared to DMSO-treated cells. Inhibition of MLKL activation did not interfere with viral replication (Fig. 9B). To confirm the activation of

MLKL following HCoV-OC43 infection, we proceeded by detecting its phosphorylated form. Indeed, phosphorylated MLKL was observed only after infection whereas in the presence of NSA, both infections showed less phosphorylation of MLKL (Fig. 9C). Following activation, MLKL is known to homo-oligomerize and to translocate to the plasma membrane, therefore we sought to evaluate if it was the case during HCoV-OC43 infection. We infected LA-N-5 cells with the reference or mutant virus and then the cells were labeled with antibody against the N-terminal epitope of MLKL, without previous membrane permeabilization to ensure that staining detected only the protein inserted into the plasma membrane with the N-terminal epitope of MLKL located on the outer side of the membrane. Confocal microscopy revealed that MLKL was at the cell surface after HCoV-OC43 infection compared to mock-infected cells (Fig. 9D) and that this translocation to the cell surface was more important after infection by the mutant virus. Together, these results indicate that MLKL is involved in neuronal cell death following HCoV-OC43 infection and that this activation is more substantial during infection by the S-mutant virus compared to wt virus.

DISCUSSION

The human coronavirus OC43 (HCoV-OC43) has been demonstrated to be more than just a respiratory pathogen as it possesses neuroinvasive and neurotropic properties, which raises the interest to study the potential relationship between HCoV-OC43 and neurological disease (10, 11). In the current study, we demonstrated that neurovirulent HCoV-OC43 infection leads to a neuronal response associated with the activation of regulated cell death (RCD). Moreover, two point mutations in the spike (S) glycoprotein (H183R and Y241H) are sufficient to accelerate viral dissemination as well as neuronal cell death. Accordingly, we introduced these mutations in the infectious cDNA clone of HCoV-OC43 (pBAC-OC43^{FL}) to produce a recombinant mutated rOC/U$_{s183\text{-}241}$ virus. Activation of necroptosis-like pathway may represent a neuronal response to HCoV-OC43 infection to limit viral propagation, but could also result in deleterious consequences associated with neuronal loss and neuropathology in the infected host.

Several neurotropic viruses such as HIV, HSV-1 and Influenza A virus (IAV) were reported to induce neuronal insults such as protein aggregates, oxidative stress, ER stress and synaptic alterations during infection, all contributing to neuropathogenesis (49-51). Indeed, neurons in the CNS are particularly vulnerable to intracellular dysfunction where protein misfolding or synaptic alterations could result in neuronal loss (52-55). Our previous studies demonstrated that rOC/U$_{s183\text{-}241}$ infection enhanced the unfolded protein response (UPR) and protein synthesis inhibition (13), suggesting that this mutant virus could increase ER stress in neurons associated with neurodegeneration and neuropathogenesis in infected mice. These observations can also relate to other data, which demonstrated that HCoV-OC43 interferes with neurotransmitter homeostasis and

induces glutamate excitotoxicity (15, 16), thus promoting neuronal stress and eventual neuropathogenesis in infected mice.

Herein, our results indicate that the S-mutant rOC/$U_{s183-241}$ acquired the capacity to disseminate more rapidly and to produce more infectious particles than the reference virus in the CNS of infected mice as well as in neuronal cell cultures, resulting in an increased neurovirulence and induction of cell-death (Figs. 1-4). Moreover, mutations in the viral S protein appear to modulate the neuronal cellular response involving inflammation, neuronal damage and eventually loss of neurons by RCD activation as seen in other viral infection such as MHV, HSV-1 and flavivirus, (56-58). Indeed, RCD is sometimes known to favor a pro-inflammatory environment and contribute to neuroinflammation by mediating the release of damage-associated molecular pattern (DAMPs) and production of pro-inflammatory cytokines (59, 60). We previously reported that HCoV-OC43 infection leads to the production of pro-inflammatory cytokines such as IL-1, TNFα, IL-6 and T-lymphocytes infiltration (CD4+ and CD8+) in the CNS (17). This, together with the increased astrogliosis observed in the CNS of S mutant-infected mice (Fig. 2B), suggest that infection by this mutant virus could contribute to enhance pro-inflammatory cytokine secretion and to a deleterious neuroinflammation process. Similarly, neurovirulence of the murine coronavirus MHV-A59 was linked to the excessive production of pro-inflammatory cytokines by astrocytes and microglial cells in brain and spinal cord of infected mice (61).

Apart from activation of neuroinflammation and neuronal damage, RCD activation during HCoV-OC43 infection could also serve to restrict the pathogen spread. We previously demonstrated that HCoV-OC43 infection induced neuronal cell death in the

mouse CNS (11). Despite the lack of precise identification of RCD, these results suggest that, while contributing to the elimination of infected neurons, RCD could participate in virus-initiated neuropathogenesis. Our data on neuronal cell death indicate that the infection by the mutant virus induces more neuronal cell death (Fig. 4). Surprisingly, even though we previously showed relocalization of the Bax protein to the mitochondria (14) and considering that the murine counterpart of HCoV-OC43, the mouse hepatitis virus (MHV), was reported to induce Bax-dependent apoptosis in oligodendrocytes (62, 63), the pro-apoptotic cellular factor Bax was not involved in neuronal cell death induced by HCoV-OC43. This suggests that during a coronavirus infection, this pro-apoptotic factor could be activated in a cell-type specific manner or that the human virus possesses specific strategies to subvert Bax-dependent apoptosis and evade this type of RCD activation. Although Bax-dependent apoptosis is often activated during infection in order to limit viral propagation (64-66), several viruses had acquired diverse strategies to block this form of RCD (67). Indeed, cytomegalovirus (68), myxoma virus (69), vaccinia virus (70) and Epstein-Barr virus (71) all encode viral Bcl-2 homologs that interact with and inhibit Bax activation. Until now, no HCoV-OC43 proteins have been shown to have anti-apoptotic properties and further studies are warranted to explore how HCoV-OC43 could interfere with Bax-dependent apoptosis in neuronal cells. On the other hand, it was already reported that some intracellular oxidative alterations could results in translocation of Bax to the mitochondria without any signs of apoptosis activation (72). As several viruses are known to destabilize cellular redox state during infection (73-75), it is possible that HCoV-OC43 infection induces a redox imbalance, promoting translocation of Bax to the mitochondria without any consequences on neuronal cell death.

Other types of RCD are now well described and are activated by different stimuli (21). Necroptosis is now considered as an alternative RCD pathway mostly involved when caspase-8 dependent apoptosis is inhibited or altered or when endogenous RIP3 expression is high enough to sensitize cells to necroptosis activation (76). Moreover, many neurological disorders, such as amyotrophic lateral sclerosis (77), Huntington's disease (78), multiple sclerosis (79) and ischemic brain injury (80) may be related to necroptosis activation as observed by a significant expression or activity of RIP1, RIP3 and MLKL (81). The expression and activation of these factors are also considered to be a defense mechanism against pathogen invasion (67, 82). Several viruses, such as HIV (83), reovirus (84), IAV (85), CMV and HSV (86) are known to engage activation of RIP1, RIP3 or MLKL in infected cells with HSV-1 and HSV-2, and CMV being able to interfere with necroptosis to block cell death (87, 88). Our results show that infection of neuronal cultures by the S-mutant virus leads to an increase in RIP1 and RIP3 transcription compared to wt virus. As the S-mutant virus is disseminating faster, this could be due to an increased number of infected neurons that are engaging a pro-necroptotic response but also to the fact that these mutant-infected cells produce more infectious particles (Fig. 4 and ref 13), which could induce a more intense disruption of the cell homeostasis and, in the end, trigger a stronger activation of RIP1 and RIP3. Furthermore, as previously suggested (14), the faster spreading and increased production of viral particles by the S-mutant virus may also implicate other viral factors involved in the regulation of RCD that are produced in larger amount compared to wild-type virus, as well as other host-cell factors. Even though there were no corresponding increased amounts of the RIP proteins, our results clearly indicate that RIP1-associated RCD plays a role in HCoV-induced cell death as seen by a significant increased survival of infected LA-N-5 cells in which RIP1

has been knocked-down (Fig. 8B) Moreover, inhibition of RIP1 expression also results in an increase of cell-associated infectious particles production (Fig. 8C), suggesting that RIP1 is potentially activated by neurons in response to the infection as an attempt to restrict viral replication. MLKL represents the major executioner factor in the necroptotic pathway; therefore the significant increased survival of LA-N-5 cells in the presence of MLKL inhibitor (NSA) and MLKL phosphorylation and relocalization at the surface of the neurons (Fig. 9) suggest that necroptosis-like pathway related to RIP1 and MLKL were involved for the cell death induced by HCoV-OC43. Recently, Nogusa and colleagues showed that RIP3 can activate both MLKL-driven necroptosis and FADD-mediated apoptosis in IAV infected cells to restrict viral propagation and suggested that this process may do so by reducing viral replication in infected cells and promoting activation of immune cells associated with the release of DAMPs from dying cells (85). This is in accordance with our hypothesis that the necroptotic process engaged during HCoV-OC43 infection may serve to activate immunity. On the other hand, this caspase-dependent pro-apoptotic role of RIP3 during IAV infection is highly interesting, as necroptosis and apoptosis are often seen as mutually exclusive alternative forms of RCD. Considering this observation, even though Bax-mediated apoptosis (Fig. 6) and caspases (14) are clearly not involved during neuronal cell death in our model, we cannot rule out that, in parallel to necroptosis, other forms of RCD may also participate during neuronal cell infection by HCoV-OC43.

As described before (13), HCoV-OC43 induces an ER stress associated with the activation of some components of the UPR system, including GRP78. The induction of ER stress and activation of GRP78 was previously reported to precede and lead to necroptosis activation by an unknown mechanism (89, 90). Therefore, one can

hypothesize that infection by HCoV-OC43 induced an ER stress in neurons that initiate RIP1-MLKL-driven necroptosis. Furthermore, inhibition of cyclophilin D, an isomerase acting to modulate mitochondrial permeability transition pore, has been shown to reduce necroptosis-related cell death in mouse embryonic fibroblasts (91, 92). We previously reported that inhibiting cyclophilin D in HCoV-OC43-infected LA-N-5 partially protects neurons from cell death, supporting the hypothesis that this factor is also at least partially involved in RIP1-MLKL necroptosis-like pathway. In sum, HCoV-OC43-induced RCD appears to involve several host-cell factors and potential crosstalk between signalling pathways that implicate necroptosis. Further studies to continue to characterize the cascade of events that takes place during the process and whether the mutations in the viral S protein engage other pathways in infected cells are on-going.

The current study demonstrates that two point mutations located in the viral S glycoprotein are sufficient to increase the neurovirulence of HCoV-OC43 in mice. Again, by improving the capacity of the mutant virus to produce more infectious particles and disseminate more efficiently, these mutations seem to engage an increased activation of RIP1-MLKL necroptosis-like pathway. Therefore, it is reasonable to think that host-cells respond to HCoV-OC43 infection within the CNS by engaging a necroptosis-like pathway in order to clear or at least limit the infection in case when other types of RCD (like the Bax-dependent apoptosis) are unable to accomplish this function. However, when infection triggers a stronger activation of this necroptosis-like pathway (mutant vs wild type virus), it may induce an excessive neuroinflammation associated with an enhanced release of DAMPs (40, 82) and the cellular response to the infection may become deleterious for the host. Depending on the viral infection within the CNS, the neuronal responses may engage specific factors or pathways of RCD to clear the pathogens but at

the same time, generating damages that increase susceptibility to neurological disorders for the host. The challenge will be to target and modulate specific RCD activation without interfering in antiviral responses within the CNS to attenuate the deleterious effect following neuronal cell death and improve long term strategies for CNS protection against neurological diseases.

Journal of Virology JVI Journal of Virology

ACKNOWLEDGMENTS

We thank Jessie Tremblay for excellent technical assistance with confocal microscopy and Dr. Mathieu Dubé for helpful discussions.

FUNDING INFORMATION

This work was supported by Grant No. MT-9203 from the CIHR's Institute of Infection and Immunity (III) to Pierre J. Talbot, who is the holder of the Tier-1 (Senior) Canada Research Chair in Neuroimmunovirology award. Mathieu Meessen-Pinard acknowledges a doctoral studentship from the *Fonds de recherche Québec – Santé* and Alain Le Coupanec acknowledges a doctoral studentship from *Fondation Universitaire Armand-Frappier de l'INRS.*

The funders had no role in study design, data collection and interpretation, or the decision to submit the work for publication.

REFERENCES

1. **Vabret A, Dina J, Brison E, Brouard J, Freymuth F.** 2009. [Human coronaviruses]. Pathol Biol (Paris) **57:**149-160.
2. **Forgie S, Marrie TJ.** 2009. Healthcare-associated atypical pneumonia. Semin Respir Crit Care Med **30:**67-85.
3. **Riski H, Hovi T.** 1980. Coronavirus infections of man associated with diseases other than the common cold. J Med Virol **6:**259-265.
4. **Yeh EA, Collins A, Cohen ME, Duffner PK, Faden H.** 2004. Detection of coronavirus in the central nervous system of a child with acute disseminated encephalomyelitis. Pediatrics **113:**e73-76.
5. **McGavern DB, Kang SS.** 2011. Illuminating viral infections in the nervous system. Nat Rev Immunol **11:**318-329.
6. **Arabi YM, Harthi A, Hussein J, Bouchama A, Johani S, Hajeer AH, Saeed BT, Wahbi A, Saedy A, AlDabbagh T, Okaili R, Sadat M, Balkhy H.** 2015. Severe neurologic syndrome associated with Middle East respiratory syndrome corona virus (MERS-CoV). Infection **43:**495-501.
7. **Morfopoulou S, Brown JR, Davies EG, Anderson G, Virasami A, Qasim W, Chong WK, Hubank M, Plagnol V, Desforges M, Jacques TS, Talbot PJ, Breuer J.** 2016. Human Coronavirus OC43 Associated with Fatal Encephalitis. N Engl J Med **375:**497-498.
8. **Buchmeier MJ, Dalziel RG, Koolen MJ, Lampert PW.** 1987. Molecular determinants of CNS virulence of MHV-4. Adv Exp Med Biol **218:**287-295.
9. **Hosking MP, Lane TE.** 2010. The Pathogenesis of Murine Coronavirus Infection of the Central Nervous System. Critical Reviews in Immunology **30:**119-130.

10. **Jacomy H, Talbot PJ.** 2003. Vacuolating encephalitis in mice infected by human coronavirus OC43. Virology **315:**20-33.

11. **Jacomy H, Fragoso G, Almazan G, Mushynski WE, Talbot PJ.** 2006. Human coronavirus OC43 infection induces chronic encephalitis leading to disabilities in BALB/C mice. Virology **349:**335-346.

12. **Arbour N, Day R, Newcombe J, Talbot PJ.** 2000. Neuroinvasion by human respiratory coronaviruses. J Virol **74:**8913-8921.

13. **Favreau DJ, Desforges M, St-Jean JR, Talbot PJ.** 2009. A human coronavirus OC43 variant harboring persistence-associated mutations in the S glycoprotein differentially induces the unfolded protein response in human neurons as compared to wild-type virus. Virology **395:**255-267.

14. **Favreau DJ, Meessen-Pinard M, Desforges M, Talbot PJ.** 2012. Human coronavirus-induced neuronal programmed cell death is cyclophilin d dependent and potentially caspase dispensable. J Virol **86:**81-93.

15. **Brison E, Jacomy H, Desforges M, Talbot PJ.** 2011. Glutamate excitotoxicity is involved in the induction of paralysis in mice after infection by a human coronavirus with a single point mutation in its spike protein. J Virol **85:**12464-12473.

16. **Brison E, Jacomy H, Desforges M, Talbot PJ.** 2014. Novel treatment with neuroprotective and antiviral properties against a neuroinvasive human respiratory virus. J Virol **88:**1548-1563.

17. **Jacomy H, St-Jean JR, Brison E, Marceau G, Desforges M, Talbot PJ.** 2010. Mutations in the spike glycoprotein of human coronavirus OC43 modulate disease

in BALB/c mice from encephalitis to flaccid paralysis and demyelination. J Neurovirol **16:**279-293.

18. **Linkermann A, Stockwell BR, Krautwald S, Anders HJ.** 2014. Regulated cell death and inflammation: an auto-amplification loop causes organ failure. Nat Rev Immunol **14:**759-767.

19. **Upton JW, Chan FK.** 2014. Staying Alive: Cell Death in Antiviral Immunity. Mol Cell **54:**273-280.

20. **Galluzzi L, Brenner C, Morselli E, Touat Z, Kroemer G.** 2008. Viral control of mitochondrial apoptosis. PLoS Pathog **4:**e1000018.

21. **Galluzzi L, Vitale I, Abrams JM, Alnemri ES, Baehrecke EH, Blagosklonny MV, Dawson TM, Dawson VL, El-Deiry WS, Fulda S, Gottlieb E, Green DR, Hengartner MO, Kepp O, Knight RA, Kumar S, Lipton SA, Lu X, Madeo F, Malorni W, Mehlen P, Nunez G, Peter ME, Piacentini M, Rubinsztein DC, Shi Y, Simon HU, Vandenabeele P, White E, Yuan J, Zhivotovsky B, Melino G, Kroemer G.** 2012. Molecular definitions of cell death subroutines: recommendations of the Nomenclature Committee on Cell Death 2012. Cell Death Differ **19:**107-120.

22. **Wajant H, Pfizenmaier K, Scheurich P.** 2003. Tumor necrosis factor signaling. Cell Death Differ **10:**45-65.

23. **Seol DW, Li J, Seol MH, Park SY, Talanian RV, Billiar TR.** 2001. Signaling events triggered by tumor necrosis factor-related apoptosis-inducing ligand (TRAIL): caspase-8 is required for TRAIL-induced apoptosis. Cancer Res **61:**1138-1143.

24. **Lettau M, Paulsen M, Schmidt H, Janssen O.** 2011. Insights into the molecular regulation of FasL (CD178) biology. Eur J Cell Biol **90:**456-466.

25. **Feoktistova M, Geserick P, Panayotova-Dimitrova D, Leverkus M.** 2012. Pick your poison: The Ripoptosome, a cell death platform regulating apoptosis and necroptosis. Cell Cycle **11:**460-467.

26. **Meylan E, Tschopp J.** 2005. The RIP kinases: crucial integrators of cellular stress. Trends Biochem Sci **30:**151-159.

27. **Dunai Z, Bauer PI, Mihalik R.** 2011. Necroptosis: biochemical, physiological and pathological aspects. Pathol Oncol Res **17:**791-800.

28. **Christofferson DE, Li Y, Hitomi J, Zhou W, Upperman C, Zhu H, Gerber SA, Gygi S, Yuan J.** 2012. A novel role for RIP1 kinase in mediating TNFalpha production. Cell Death Dis **3:**e320.

29. **Cho YS, Challa S, Moquin D, Genga R, Ray TD, Guildford M, Chan FK.** 2009. Phosphorylation-driven assembly of the RIP1-RIP3 complex regulates programmed necrosis and virus-induced inflammation. Cell **137:**1112-1123.

30. **Zhang YY, Liu H.** 2013. Connections Between Various Trigger Factors and the RIP1/ RIP3 Signaling Pathway Involved in Necroptosis. Asian Pac J Cancer Prev **14:**7069-7074.

31. **Baines CP.** 2010. Role of the mitochondrion in programmed necrosis. Front Physiol **1:**156.

32. **Cai Z, Jitkaew S, Zhao J, Chiang HC, Choksi S, Liu J, Ward Y, Wu LG, Liu ZG.** 2014. Plasma membrane translocation of trimerized MLKL protein is required for TNF-induced necroptosis. Nat Cell Biol **16:**55-65.

731 33. **Chen X, Li W, Ren J, Huang D, He WT, Song Y, Yang C, Li W, Zheng X,**
732 **Chen P, Han J.** 2014. Translocation of mixed lineage kinase domain-like protein
733 to plasma membrane leads to necrotic cell death. Cell Res **24:**105-121.
734 34. **Hill DP, Robertson KA.** 1998. Differentiation of LA-N-5 neuroblastoma cells
735 into cholinergic neurons: methods for differentiation, immunohistochemistry and
736 reporter gene introduction. Brain Res Brain Res Protoc **2:**183-190.
737 35. **St-Jean JR, Desforges M, Almazan F, Jacomy H, Enjuanes L, Talbot PJ.**
738 2006. Recovery of a neurovirulent human coronavirus OC43 from an infectious
739 cDNA clone. J Virol **80:**3670-3674.
740 36. **Le Coupanec A, Desforges M, Meessen-Pinard M, Dube M, Day R, Seidah**
741 **NG, Talbot PJ.** 2015. Cleavage of a Neuroinvasive Human Respiratory Virus
742 Spike Glycoprotein by Proprotein Convertases Modulates Neurovirulence and
743 Virus Spread within the Central Nervous System. PLoS Pathog **11:**e1005261.
744 37. **Lambert F, Jacomy H, Marceau G, Talbot PJ.** 2008. Titration of human
745 coronaviruses, HcoV-229E and HCoV-OC43, by an indirect immunoperoxidase
746 assay. Methods Mol Biol **454:**93-102.
747 38. **Miyashita T, Krajewski S, Krajewska M, Wang HG, Lin HK, Liebermann**
748 **DA, Hoffman B, Reed JC.** 1994. Tumor suppressor p53 is a regulator of bcl-2
749 and bax gene expression in vitro and in vivo. Oncogene **9:**1799-1805.
750 39. **Miyashita T, Reed JC.** 1995. Tumor suppressor p53 is a direct transcriptional
751 activator of the human bax gene. Cell **80:**293-299.
752 40. **Sharif-Askari E, Nakhaei P, Oliere S, Tumilasci V, Hernandez E, Wilkinson**
753 **P, Lin R, Bell J, Hiscott J.** 2007. Bax-dependent mitochondrial membrane

754 permeabilization enhances IRF3-mediated innate immune response during VSV
755 infection. Virology **365:**20-33.
756 41. **Xu W, Jing L, Wang Q, Lin CC, Chen X, Diao J, Liu Y, Sun X.** 2015. Bax-
757 PGAM5L-Drp1 complex is required for intrinsic apoptosis execution. Oncotarget.
758 42. **Vanlangenakker N, Vanden Berghe T, Vandenabeele P.** 2012. Many stimuli
759 pull the necrotic trigger, an overview. Cell Death Differ **19:**75-86.
760 43. **Degterev A, Huang Z, Boyce M, Li Y, Jagtap P, Mizushima N, Cuny GD,**
761 **Mitchison TJ, Moskowitz MA, Yuan J.** 2005. Chemical inhibitor of
762 nonapoptotic cell death with therapeutic potential for ischemic brain injury. Nat
763 Chem Biol **1:**112-119.
764 44. **King MD, Whitaker-Lea WA, Campbell JM, Alleyne CH, Jr., Dhandapani**
765 **KM.** 2014. Necrostatin-1 reduces neurovascular injury after intracerebral
766 hemorrhage. Int J Cell Biol **2014:**495817.
767 45. **Upton JW, Kaiser WJ, Mocarski ES.** 2012. DAI/ZBP1/DLM-1 Complexes with
768 RIP3 to Mediate Virus-Induced Programmed Necrosis that Is Targeted by Murine
769 Cytomegalovirus vIRA. Cell Host Microbe **11:**290-297.
770 46. **Mack C, Sickmann A, Lembo D, Brune W.** 2008. Inhibition of proinflammatory
771 and innate immune signaling pathways by a cytomegalovirus RIP1-interacting
772 protein. Proc Natl Acad Sci U S A **105:**3094-3099.
773 47. **Chien H, Dix RD.** 2012. Evidence for multiple cell death pathways during
774 development of experimental cytomegalovirus retinitis in mice with retrovirus-
775 induced immunosuppression: apoptosis, necroptosis, and pyroptosis. J Virol
776 **86:**10961-10978.

48. **Dondelinger Y, Declercq W, Montessuit S, Roelandt R, Goncalves A, Bruggeman I, Hulpiau P, Weber K, Sehon CA, Marquis RW, Bertin J, Gough PJ, Savvides S, Martinou JC, Bertrand MJ, Vandenabeele P.** 2014. MLKL compromises plasma membrane integrity by binding to phosphatidylinositol phosphates. Cell Rep **7:**971-981.

49. **Xu J, Ikezu T.** 2009. The comorbidity of HIV-associated neurocognitive disorders and Alzheimer's disease: a foreseeable medical challenge in post-HAART era. J Neuroimmune Pharmacol **4:**200-212.

50. **Brask J, Chauhan A, Hill RH, Ljunggren HG, Kristensson K.** 2005. Effects on synaptic activity in cultured hippocampal neurons by influenza A viral proteins. J Neurovirol **11:**395-402.

51. **Kavouras JH, Prandovszky E, Valyi-Nagy K, Kovacs SK, Tiwari V, Kovacs M, Shukla D, Valyi-Nagy T.** 2007. Herpes simplex virus type 1 infection induces oxidative stress and the release of bioactive lipid peroxidation by-products in mouse P19N neural cell cultures. J Neurovirol **13:**416-425.

52. **Soto C.** 2003. Unfolding the role of protein misfolding in neurodegenerative diseases. Nat Rev Neurosci **4:**49-60.

53. **Butterfield DA, Reed T, Newman SF, Sultana R.** 2007. Roles of amyloid beta-peptide-associated oxidative stress and brain protein modifications in the pathogenesis of Alzheimer's disease and mild cognitive impairment. Free Radic Biol Med **43:**658-677.

54. **Mattson MP.** 2003. Excitotoxic and excitoprotective mechanisms: abundant targets for the prevention and treatment of neurodegenerative disorders. Neuromolecular Med **3:**65-94.

55. **Schondorf DC, Aureli M, McAllister FE, Hindley CJ, Mayer F, Schmid B, Sardi SP, Valsecchi M, Hoffmann S, Schwarz LK, Hedrich U, Berg D, Shihabuddin LS, Hu J, Pruszak J, Gygi SP, Sonnino S, Gasser T, Deleidi M.** 2014. iPSC-derived neurons from GBA1-associated Parkinson's disease patients show autophagic defects and impaired calcium homeostasis. Nat Commun **5:**4028.

56. **Das Sarma J, Kenyon LC, Hingley ST, Shindler KS.** 2009. Mechanisms of primary axonal damage in a viral model of multiple sclerosis. J Neurosci **29:**10272-10280.

57. **Zambrano A, Solis L, Salvadores N, Cortes M, Lerchundi R, Otth C.** 2008. Neuronal cytoskeletal dynamic modification and neurodegeneration induced by infection with herpes simplex virus type 1. J Alzheimers Dis **14:**259-269.

58. **Leyssen P, Paeshuyse J, Charlier N, Van Lommel A, Drosten C, De Clercq E, Neyts J.** 2003. Impact of direct virus-induced neuronal dysfunction and immunological damage on the progression of flavivirus (Modoc) encephalitis in a murine model. J Neurovirol **9:**69-78.

59. **Kaczmarek A, Vandenabeele P, Krysko DV.** 2013. Necroptosis: the release of damage-associated molecular patterns and its physiological relevance. Immunity **38:**209-223.

60. **Pasparakis M, Vandenabeele P.** 2015. Necroptosis and its role in inflammation. Nature **517:**311-320.

61. **Li Y, Fu L, Gonzales DM, Lavi E.** 2004. Coronavirus neurovirulence correlates with the ability of the virus to induce proinflammatory cytokine signals from astrocytes and microglia. J Virol **78:**3398-3406.

824 62. **Liu Y, Pu Y, Zhang X.** 2006. Role of the mitochondrial signaling pathway in
825 murine coronavirus-induced oligodendrocyte apoptosis. J Virol **80:**395-403.
826 63. **Liu Y, Zhang X.** 2007. Murine coronavirus-induced oligodendrocyte apoptosis is
827 mediated through the activation of the Fas signaling pathway. Virology **360:**364-
828 375.
829 64. **Parquet MC, Kumatori A, Hasebe F, Morita K, Igarashi A.** 2001. West Nile
830 virus-induced bax-dependent apoptosis. FEBS Lett **500:**17-24.
831 65. **Deng L, Adachi T, Kitayama K, Bungyoku Y, Kitazawa S, Ishido S, Shoji I,**
832 **Hotta H.** 2008. Hepatitis C virus infection induces apoptosis through a Bax-
833 triggered, mitochondrion-mediated, caspase 3-dependent pathway. J Virol
834 **82:**10375-10385.
835 66. **Castedo M, Ferri KF, Blanco J, Roumier T, Larochette N, Barretina J,**
836 **Amendola A, Nardacci R, Metivier D, Este JA, Piacentini M, Kroemer G.**
837 2001. Human immunodeficiency virus 1 envelope glycoprotein complex-induced
838 apoptosis involves mammalian target of rapamycin/FKBP12-rapamycin-associated
839 protein-mediated p53 phosphorylation. J Exp Med **194:**1097-1110.
840 67. **Lytvyn DIB, Ya. B.; Desforges, M.; Meessen-Pinard, M.; Talbot, P.J.;**
841 **Sabater, B. and Martin, M. .** 2016. Modulating regulated cell death: the virus
842 way to influence cell fate, survive and persist. *In* Rice J (ed), Programmed cell
843 death in plants and animals. Nova science publishers, New York.
844 68. **Poncet D, Pauleau AL, Szabadkai G, Vozza A, Scholz SR, Le Bras M, Briere**
845 **JJ, Jalil A, Le Moigne R, Brenner C, Hahn G, Wittig I, Schagger H, Lemaire**
846 **C, Bianchi K, Souquere S, Pierron G, Rustin P, Goldmacher VS, Rizzuto R,**

Palmieri F, Kroemer G. 2006. Cytopathic effects of the cytomegalovirus-encoded apoptosis inhibitory protein vMIA. J Cell Biol **174:**985-996.

69. **Su J, Wang G, Barrett JW, Irvine TS, Gao X, McFadden G.** 2006. Myxoma virus M11L blocks apoptosis through inhibition of conformational activation of Bax at the mitochondria. J Virol **80:**1140-1151.

70. **Cooray S, Bahar MW, Abrescia NG, McVey CE, Bartlett NW, Chen RA, Stuart DI, Grimes JM, Smith GL.** 2007. Functional and structural studies of the vaccinia virus virulence factor N1 reveal a Bcl-2-like anti-apoptotic protein. J Gen Virol **88:**1656-1666.

71. **Marshall WL, Yim C, Gustafson E, Graf T, Sage DR, Hanify K, Williams L, Fingeroth J, Finberg RW.** 1999. Epstein-Barr virus encodes a novel homolog of the bcl-2 oncogene that inhibits apoptosis and associates with Bax and Bak. J Virol **73:**5181-5185.

72. **D'Alessio M, De Nicola M, Coppola S, Gualandi G, Pugliese L, Cerella C, Cristofanon S, Civitareale P, Ciriolo MR, Bergamaschi A, Magrini A, Ghibelli L.** 2005. Oxidative Bax dimerization promotes its translocation to mitochondria independently of apoptosis. FASEB J **19:**1504-1506.

73. **Garofalo RP, Kolli D, Casola A.** 2013. Respiratory syncytial virus infection: mechanisms of redox control and novel therapeutic opportunities. Antioxid Redox Signal **18:**186-217.

74. **Kumar S, Misra UK, Kalita J, Khanna VK, Khan MY.** 2009. Imbalance in oxidant/antioxidant system in different brain regions of rat after the infection of Japanese encephalitis virus. Neurochem Int **55:**648-654.

75. **Nakamura H, Masutani H, Yodoi J.** 2002. Redox imbalance and its control in HIV infection. Antioxid Redox Signal **4:**455-464.

76. **Han J, Zhong CQ, Zhang DW.** 2011. Programmed necrosis: backup to and competitor with apoptosis in the immune system. Nat Immunol **12:**1143-1149.

77. **Re DB, Le Verche V, Yu C, Amoroso MW, Politi KA, Phani S, Ikiz B, Hoffmann L, Koolen M, Nagata T, Papadimitriou D, Nagy P, Mitsumoto H, Kariya S, Wichterle H, Henderson CE, Przedborski S.** 2014. Necroptosis drives motor neuron death in models of both sporadic and familial ALS. Neuron **81:**1001-1008.

78. **Zhu S, Zhang Y, Bai G, Li H.** 2011. Necrostatin-1 ameliorates symptoms in R6/2 transgenic mouse model of Huntington's disease. Cell Death Dis **2:**e115.

79. **Ofengeim D, Ito Y, Najafov A, Zhang YY, Shan B, DeWitt JP, Ye JY, Zhang XM, Chang AS, Vakifahmetoglu-Norberg H, Geng JF, Py B, Zhou W, Amin P, Lima JB, Qi CT, Yu Q, Trapp B, Yuan JY.** 2015. Activation of Necroptosis in Multiple Sclerosis. Cell Reports **10:**1836-1849.

80. **Askalan R, Gabarin N, Armstrong EA, Fang Liu Y, Couchman D, Yager JY.** 2015. Mechanisms of Neurodegeneration after Severe Hypoxic-Ischemic Injury in the Neonatal Rat Brain. Brain Res doi:10.1016/j.brainres.2015.10.020.

81. **Jouan-Lanhouet S, Riquet F, Duprez L, Vanden Berghe T, Takahashi N, Vandenabeele P.** 2014. Necroptosis, in vivo detection in experimental disease models. Semin Cell Dev Biol **35:**2-13.

82. **Zhou W, Yuan J.** 2014. Necroptosis in health and diseases. Semin Cell Dev Biol **35:**14-23.

83. **Pan T, Wu S, He X, Luo H, Zhang Y, Fan M, Geng G, Ruiz VC, Zhang J, Mills L, Bai C, Zhang H.** 2014. Necroptosis Takes Place in Human Immunodeficiency Virus Type-1 (HIV-1)-Infected CD4+ T Lymphocytes. PLoS One **9:**e93944.

84. **Berger AK, Danthi P.** 2013. Reovirus activates a caspase-independent cell death pathway. MBio **4:**e00178-00113.

85. **Nogusa S, Thapa RJ, Dillon CP, Liedmann S, Oguin TH, 3rd, Ingram JP, Rodriguez DA, Kosoff R, Sharma S, Sturm O, Verbist K, Gough PJ, Bertin J, Hartmann BM, Sealfon SC, Kaiser WJ, Mocarski ES, Lopez CB, Thomas PG, Oberst A, Green DR, Balachandran S.** 2016. RIPK3 Activates Parallel Pathways of MLKL-Driven Necroptosis and FADD-Mediated Apoptosis to Protect against Influenza A Virus. Cell Host Microbe **20:**13-24.

86. **Wang X, Li Y, Liu S, Yu X, Li L, Shi C, He W, Li J, Xu L, Hu Z, Yu L, Yang Z, Chen Q, Ge L, Zhang Z, Zhou B, Jiang X, Chen S, He S.** 2014. Direct activation of RIP3/MLKL-dependent necrosis by herpes simplex virus 1 (HSV-1) protein ICP6 triggers host antiviral defense. Proc Natl Acad Sci U S A **111:**15438-15443.

87. **Guo H, Omoto S, Harris PA, Finger JN, Bertin J, Gough PJ, Kaiser WJ, Mocarski ES.** 2015. Herpes simplex virus suppresses necroptosis in human cells. Cell Host Microbe **17:**243-251.

88. **Omoto S, Guo H, Talekar GR, Roback L, Kaiser WJ, Mocarski ES.** 2015. Suppression of RIP3-dependent necroptosis by human cytomegalovirus. J Biol Chem **290:**11635-11648.

916 89. **Fan H, Tang HB, Kang J, Shan L, Song H, Zhu K, Wang J, Ju G, Wang YZ.**
917 2015. Involvement of endoplasmic reticulum stress in the necroptosis of
918 microglia/macrophages after spinal cord injury. Neuroscience **311:**362-373.
919 90. **Saveljeva S, Mc Laughlin SL, Vandenabeele P, Samali A, Bertrand MJ.** 2015.
920 Endoplasmic reticulum stress induces ligand-independent TNFR1-mediated
921 necroptosis in L929 cells. Cell Death Dis **6:**e1587.
922 91. **He S, Wang L, Miao L, Wang T, Du F, Zhao L, Wang X.** 2009. Receptor
923 interacting protein kinase-3 determines cellular necrotic response to TNF-alpha.
924 Cell **137:**1100-1111.
925 92. **Nakagawa T, Shimizu S, Watanabe T, Yamaguchi O, Otsu K, Yamagata H,**
926 **Inohara H, Kubo T, Tsujimoto Y.** 2005. Cyclophilin D-dependent mitochondrial
927 permeability transition regulates some necrotic but not apoptotic cell death. Nature
928 **434:**652-658.
929
930

LEGENDS TO FIGURES

Figure 1. rOC/$U_{s183-241}$ is more neurovirulent than rOC/ATCC in infected mice. Twenty-two day-old BALB/c female mice received $10^{2.5}$ $TCID_{50}$/10 µl of rOC/ATCC or rOC/$U_{s183-241}$ or PBS by the IC route. (A) Survival curves of mice in % over a period of 22 days (dpi). (B) Weight variations were measured every two days during 22 days and expressed in % of variation compared to day 0. (C) Evaluation of clinical scores (% of mice at each level of the scale) of mice infected by rOC/ATCC (left panel) or rOC/$U_{s183-241}$ (right panel). (D) Production of infectious particles was measured in the brain (left panel) and spinal cord (right panel) of infected mice. LOD represents Limit of Detection. Results are representative of two independent experiments and error bars represent standard deviation (SD). Statistical significance: *, P<0.05, ***, P<0.001.

Figure 2. rOC/$U_{s183-241}$ disseminates more rapidly in the brain and induces a stronger activation of astrocytes compared to rOC/ATCC in infected mice. Histological examination of hippocampus of 22 day-old BALB/c mice infected with $10^{2.5}$ $TCID_{50}$ of rOC/ATCC or rOC/$U_{s183-241}$ or PBS. (A) Detection of viral antigen (N protein) at 5 and 7 dpi at magnitude 40X. (B) Detection of glial fibrillary acidic protein (GFAP) in astrocytes (marker of astrogliosis) at 5 and 7 dpi at magnitude 200X.

Figure 3. rOC/$U_{s183/241}$ disseminates more rapidly than rOC/ATCC in neuronal cell cultures. Viral spreading was evaluated by immunofluorescence (IF). (A) Murine primary cultures of CNS infected at a MOI of 0.005 with both viruses at different time post-infection (hpi). Neurons (red) were strained with a mAb against microtubule-associated protein 2 (MAP2) and the S viral protein (green) was detected with a rabbit

antiserum. (B) Differentiated human neuroblastoma LA-N-5 cells infected at a MOI of 0.2 with both viruses at different times post-infection. Cells were stained with a mAb against S viral protein (green) and DAPI (blue) was used to observe nucleus. Results are representative of two independent experiments. Magnification 100X.

Figure 4. rOC/U$_{s183-241}$ infection increases neuronal cell death and produces more infectious particles compared to rOC/ATCC infection. (A and C) Murine mixed primary cultures of CNS from BALB/c mice were infected with rOC/ATCC or rOC/U$_{s183-241}$ at a MOI of 0.03. (B and D) Differentiated human neuroblastoma LA-N-5 cells were infected with rOC/ATCC or rOC/U$_{s183-241}$ at a MOI of 0.2. (A) Cell viability was measured by MTT assay at indicated time post-infection and expressed as relative percentage compared to mock-infected culture at each time. (B) Cell viability was measured by Presto Blue assay at indicated time post-infection and expressed as relative percentage compared to mock-infected cells at each time. (C) Production of infectious viral particles of free virus (upper panel) and cell-associated virus (lower panel) from mixed primary cultures of CNS (C) and LA-N-5 cells (D). Results are shown as mean ± SD of three independent experiments. Statistical significance: *, $P<0.05$, **, $P<0.01$ ***, $P<0.001$.

Figure 5. Bax gene expression is increased in neuronal cell cultures during neuronal response to HCoV-OC43 infection. (A) Level of Bax mRNA in murine mixed primary cultures of CNS (left panel) or differentiated human neuroblastoma LA-N-5 cells (right panel) infected with rOC/ATCC or rOC/U$_{s183-241}$ was measured by Quantitative Real-time PCR (qPCR) at indicated times post-infection. (B) Detection of Bax protein in murine mixed primary cultures of CNS (left panel) or differentiated human neuroblastoma

LA-N-5 cells (right panel) infected with rOC/ATCC or rOC/$U_{s183-241}$ at indicated times were determined by Western Blot analysis (WB). (A) Results are shown as mean ± SD of three independent experiments. Statistical significance: *, P<0.05, **, P<0.01 ***, P<0.001. (B) Results are representative of three independent experiments.

Figure 6. Bax-dependent apoptosis does not play a significant role in LA-N-5 cell death induced by HCoV-OC43 infection. (A-D) Human neuroblastoma LA-N-5 cells were transduced with control lentivirus (NT) or lentivirus containing either of two shRNA sequence against Bax (shRNA Bax #1 or #2). (A) mRNA and protein expression of Bax was analyzed by qPCR (left panel) and WB (right panel) respectively. (B) Images of phase-contrast microscopy corresponding to differentiated LA-N-5 cells expressing shRNA NT or Bax #1 infected with rOC/ATCC or rOC/$U_{s183-241}$ at 48 hpi or treated with staurosporine (STS) or infected with Vesicular stomatis virus (VSV) at 24 hpi. Arrows represent loss of axons or dendrites and arrowhead indicate rounding of cells. (C) LA-N-5 cells viability was measured by Presto Blue assay and expressed as relative % of viability compared to mock-infected cells at 48 hpi. (D) Cell viability was measured by Presto Blue assay and expressed as relative % of viability compared to mock-infected cells. Differentiated LA-N-5 cells transduced with the different shRNA were infected with Vesicular stomatitis virus (VSV) or treated with staurosporine (STS) for 24 hours. (A, B) Results are representative of two independent experiments. (C, D) Results are shown as mean ±SD of two independent experiments. Statistical significance: *, P<0.05, **, P<0.01 ***, P<0.001.

997 **Figure 7. HCoV-OC43 infection increases RIP1 and RIP3 gene expression.**
998 Level of RIP1 (upper panels) or RIP3 (lower panels) mRNA in murine mixed primary
999 cultures of CNS (A) or differentiated LA-N-5 cells (B) infected with rOC/ATCC or
1000 rOC/$U_{s183-241}$. Detection of RIP1, RIP3 and GAPDH proteins in murine primary cultures
1001 of CNS (C) or differentiated LA-N-5 cells (D) infected with rOC/ATCC or rOC/$U_{s183-241}$
1002 at indicated times. (A, B) Results are shown as mean ±SD of three independent
1003 experiments. Statistical significance: *, P<0.05, **, P<0.01 ***, P<0.001. (C, D) Results
1004 are representative of three independent experiments.

1005 **Figure 8. RIP1 is involved in HCoV-OC43-induced LA-N-5 cell death and**
1006 **limits production of infectious virus.** Differentiated LA-N-5 cells were transiently
1007 transduced with control lentivirus (shRNA NT) or lentivirus containing either of two
1008 shRNA sequences against RIP1 (shRNA RIP1 #1 or #2). (A) Expression of RIP1 was
1009 analyzed by qPCR (upper panel) and WB (lower panel). (B) Cell viability was measured
1010 by Presto Blue assay and expressed as relative % of viability compared to mock-infected
1011 cells at 72 hpi. (C) Production of cell-associated infectious viral particles for rOC/ATCC
1012 or rOC/$U_{s183-241}$ at indicated times post-infection. (A) Results are representative of three
1013 independent experiments. (B-C) Results are shown as mean ±SD of three independent
1014 experiments. Statistical significance: *, P<0.05, **, P<0.01 ***, P<0.001.

1015 **Figure 9. MLKL is involved in LA-N-5 cell death induced by HCoV-OC43.** (A)
1016 Differentiated LA-N-5 cells were infected with rOC/ATCC or rOC/$U_{s183-241}$ at a MOI of
1017 0.2 and then treated with 2 µM NSA or DMSO. Cell viability was measured by Presto
1018 Blue assay and expressed as relative % of viability compared to mock-infected cells at 72

hpi. (B) Production of infectious free virus (left panel) or cell-associated virus (right panel) for rOC/ATCC or rOC/$U_{s183-241}$ at indicated times post-infection. (C) Differentiated LA-N-5 cells were treated with 2 µM NSA or not (DMSO) after infection with rOC/ATCC or rOC/$U_{s183-241}$ at a MOI of 1. Phosphorylated MLKL was stained in red, viral S glycoprotein in green and nucleus in blue and observed by confocal microscopy. Scale bar, 5 µM. (D) Differentiated LA-N-5 cells were infected with rOC/ATCC or rOC/$U_{s183-241}$ at a MOI of 1. The surface distribution of MLKL (green) and nucleus (blue) were detected by confocal microscopy. Scale bar, 20 µM (A, B) Data are represented as mean ±SD and were obtained from three independent experiments. Statistical significance: ***, $P<0.001$. (C, D) Images shown are representative of two independent experiments.

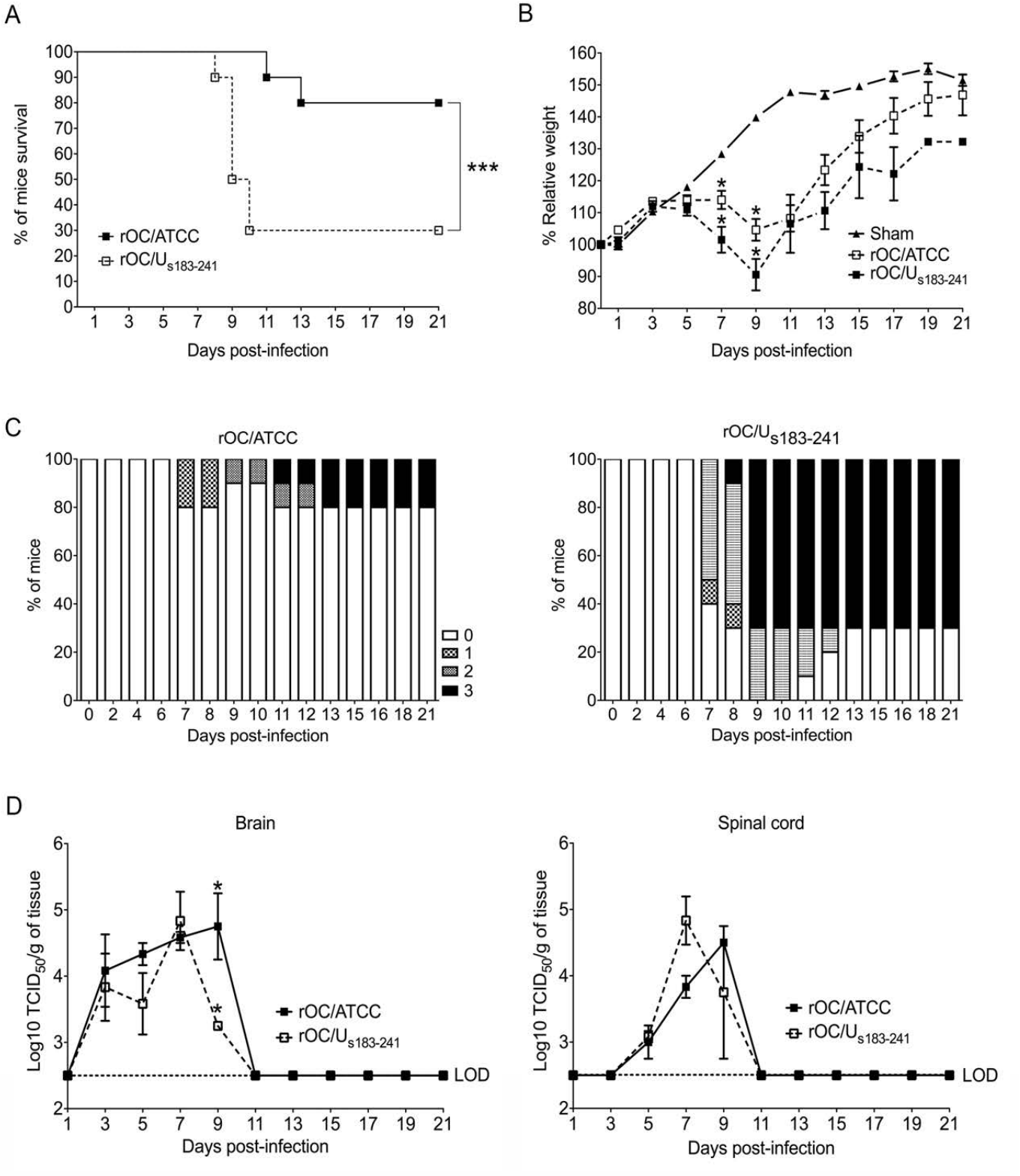

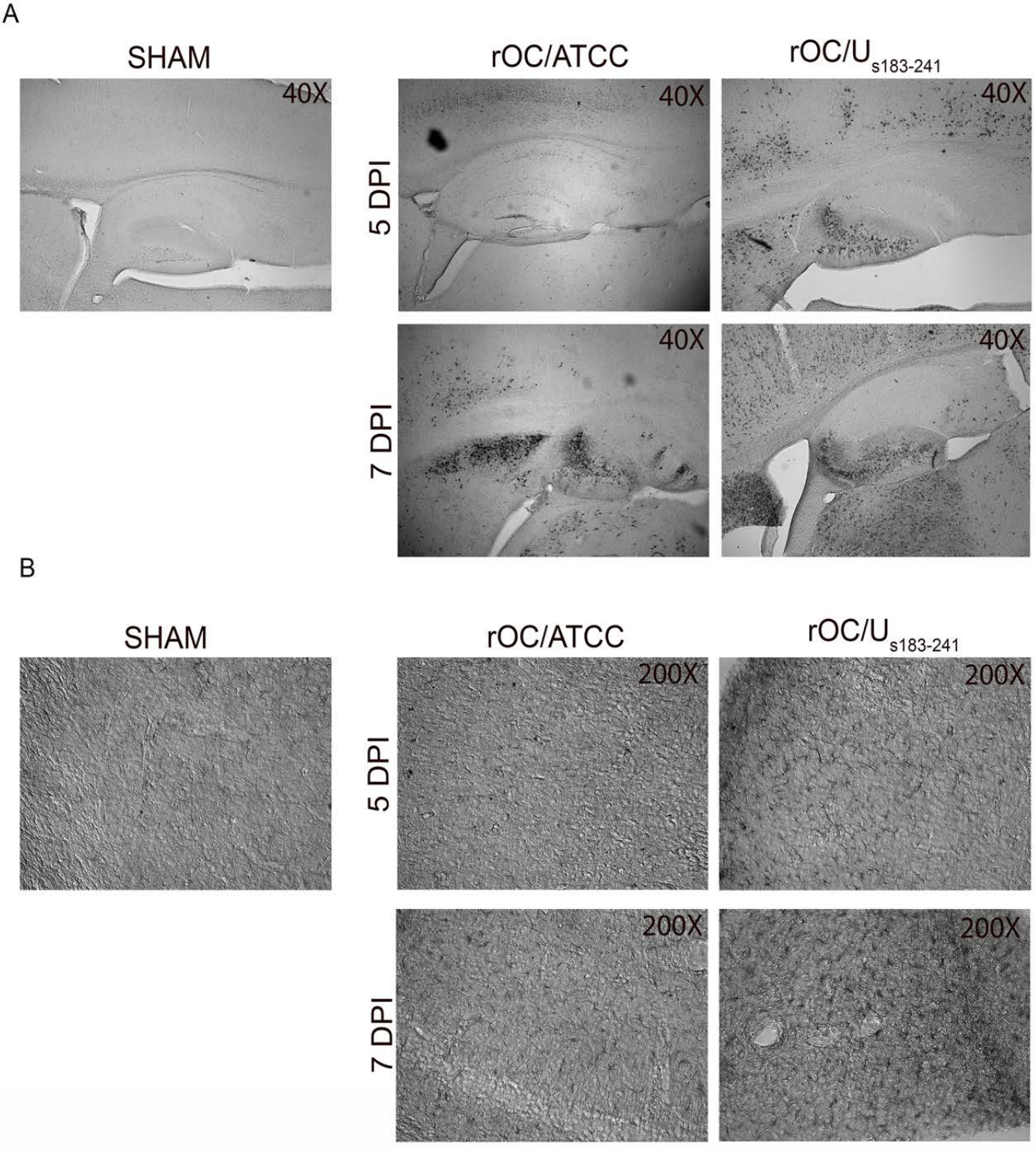

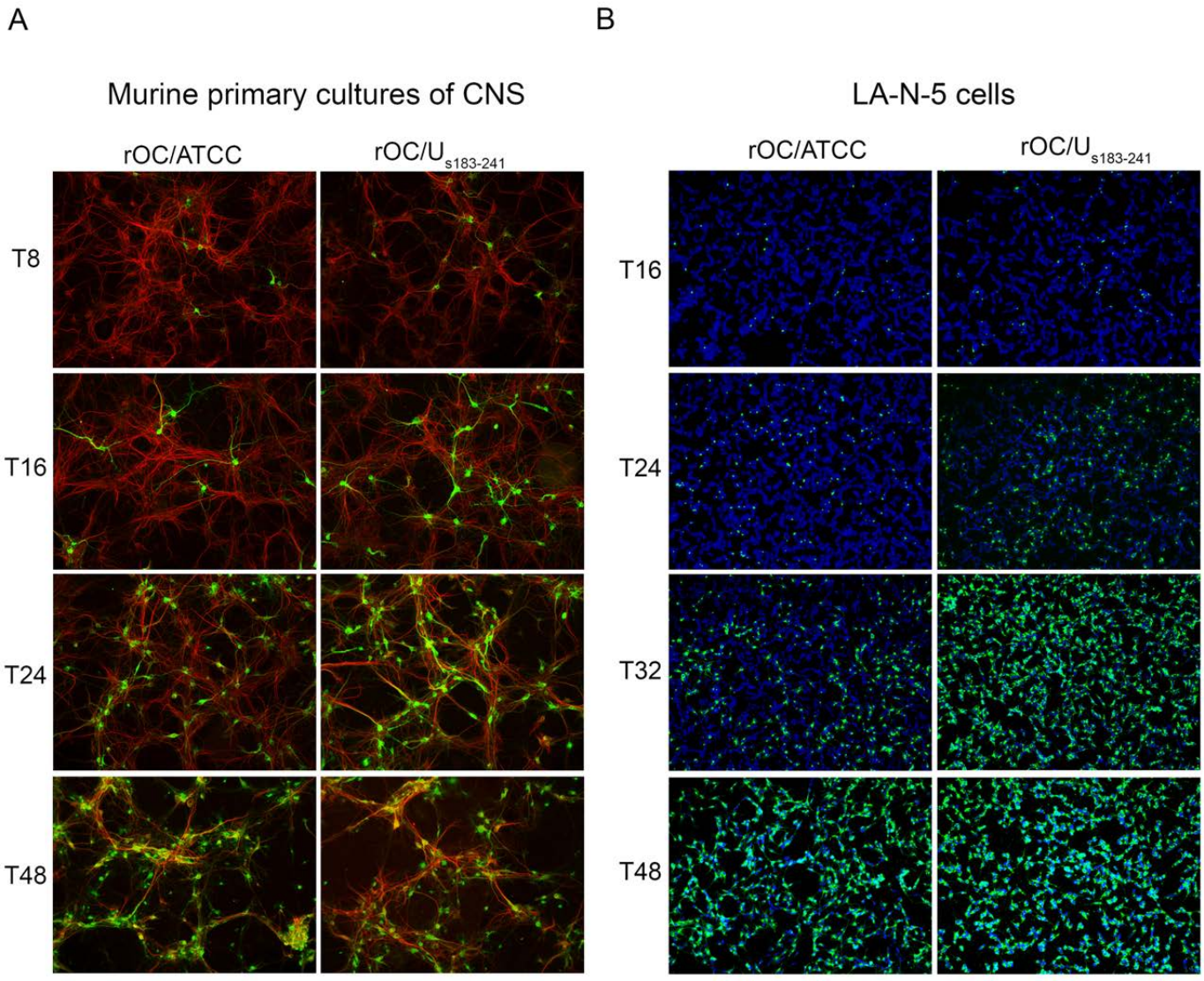

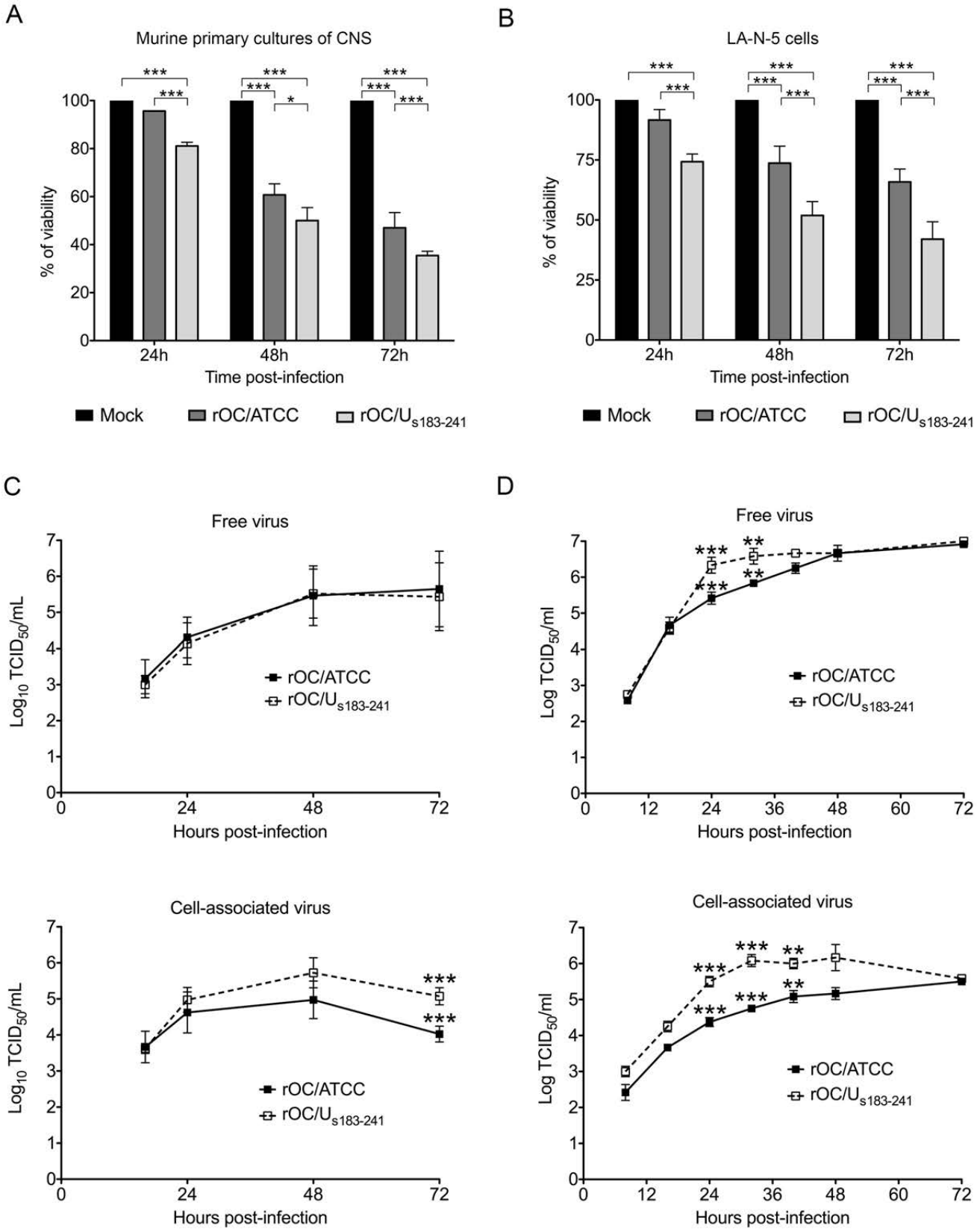

A

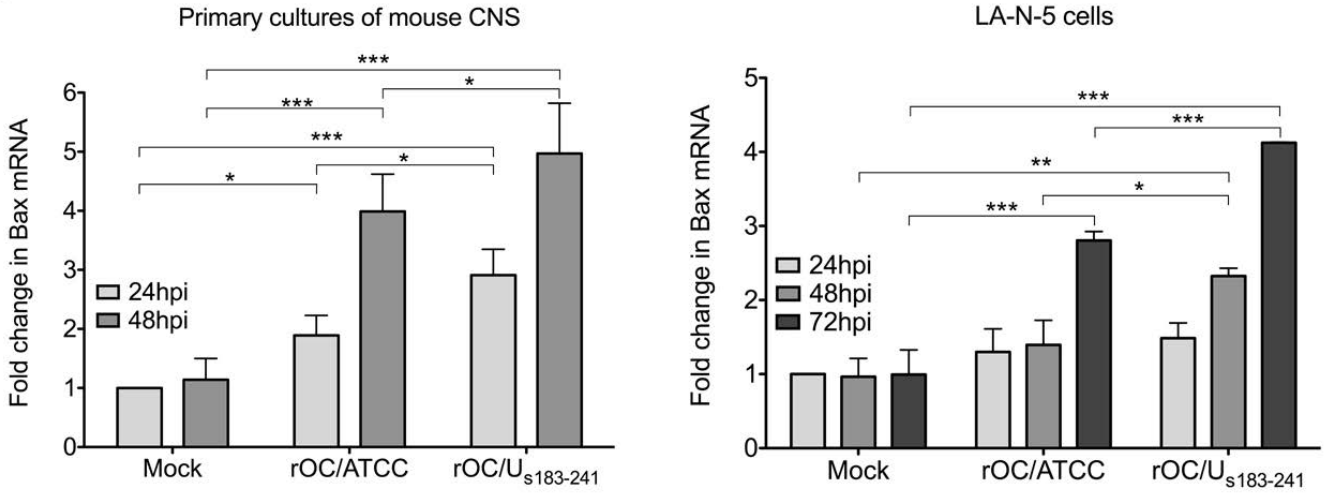

B